Journal of Alloys and Compounds, 203 (1994) 35–44
JALCOM 856

Structural study of CeM_2 (M≡Fe, Co, Ni)

A. Ślebarski, M. Matlak and M. Hafez*
Institute of Physics, Silesian University, 40-007 Katowice (Poland)

(Received January 4, 1993; in final form May 25, 1993)

Abstract

In $CeFe_2$, $CeCo_2$ and $CeNi_2$ below 100 K, measured values of the lattice constant, thermal expansion coefficient, intensities of X-ray diffraction lines (*hkl*) and resistivity exhibit similar anomalies which are closely correlated with the valence variation of the Ce ion. The intensities of the diffraction lines in the $CeCo_2$ and $CeNi_2$ samples suggest that these substances can be considered as a combination of two $MgCu_2$ structures with two different lattice constants a_1 and a_2 ($a_2<a_1$). The ratio of the numbers of crystal unit cells belonging to the two different phases is $N(a_1)/N(a_2)=9$. We endeavour to give a quantitative explanation of the abnormal variation in the Ce ion valence with temperature on the basis of the Anderson model applied to an "alloy", *i.e.* a mixture of two different phases. The anomalous behaviour of the Ce valence *vs.* temperature is also described on the basis of the phenomenological model of a "dynamic alloy".

1. Introduction

Certain rare earth (R) atoms in solids can exhibit fluctuations between two adjacent integral valence states. These valence fluctuations cause fractional occupation of the $4f^n$ and $4f^{n+1}$ configurations. Lattice constant measurement is one of the most frequently used methods to estimate the valence of non-integral valence materials. This technique assumes a linear dependence between lattice constant and valence. This procedure used for obtaining the accurate value of the valence seems to be questionable, especially for Ce, owing to the fact that (i) the hypothetical tetravalent lattice constant is unknown and (ii) the valence–volume relationship of R systems with fractional valence is non-linear because of the existence of strain energy [1] leading to visible differences between the bulk moduli of the two different valence states. However, this method is useful for investigating the relative changes in Ce ion valence as a function of T. The valence of Ce often shows a temperature dependence between 300 K and liquid helium temperature, though this dependence is relatively small. The absolute change in the valence of Ce, Δv, investigated as a function of T, *e.g.* in $CeCu_2Si_2$, $CeCu_6$ and $CeAl_3$ [2], is not larger than 0.01. These temperature dependences of the valences exhibit characteristic non-linearities which may be related *e.g.* to resistivity anomalies [2]. Röhler [2] suggests that they reflect the various crystal field schemes of the $4f^1$ Hund rule ground states.

In ref. 3 Pott *et al.* try to extract the valence of Yb in YbPd and its temperature dependence from lattice constant and thermal expansion anomalies. Below about 110 K the values differ substantially from those obtained from L_{III} absorption edges. The falsification of the valence determination via the volume anomaly in YbPd is probably due to the strong temperature dependence of the fluctuation temperature [3]; however, the two valence measurements show a similar temperature character below about 130 K. X-ray absorption spectroscopy (XAS) at the L_{III} edge has been widely used to study intermediate valent materials. In mixed valent rare earth systems a characteristic double-white-line feature is associated with the presence of $2p^54f^1$ and $2p^54f^0$ states and the average valence is simply obtained from the relative intensity of the two edges. In ref. 4, L_{III} edge spectroscopy on intermediate valent compounds is discussed in the framework of the single-impurity model. It was shown in ref. 4 that although the ratio of the intensities of the two structures at the L_{III} edge is not rigorously equal to the 4f occupation number, the respective intensities of these structures are nevertheless proportional to the 4f occupation number and thus reflect the electronic configuration in the ground state. The L_{III} edge gives room temperature values of the valence of Ce ions in CeM_2 as 3.30, 3.27 and 3.26 for M≡Fe, Co and Ni respectively [2].

In this paper we study the structural properties of the strongly mixed valent CeM_2 compounds (M≡Fe,

*Permanent address: Department of Physics, Faculty of Sciences, Suez Canal University, Ismailia, Egypt.

SSDI 0925-8388(93)00856-T

Co, Ni). The most important result presented here is the abnormal temperature dependence of the lattice parameter of CeM_2 (M ≡ Fe, Co, Ni). This effect appears to be closely correlated with other abnormal phenomena, also presented here, such as the temperature dependence of the thermal expansion coefficient, the intensity anomaly of the Bragg (*hkl*) lines and the resistivity anomaly. The measured anomalies in our opinion should have a common origin, but it is difficult to establish a common mechanism describing them adequately.

The appearance of additional diffraction lines suggests that the $CeNi_2$ sample contains two phases with the same crystal structure but with different lattice constants. In $CeCo_2$ the Bragg lines of the diffraction pattern are distinctly asymmetrical at room temperature and below, but in $CeFe_2$ all the diffraction lines become clearly asymmetrical below 200 K. Assuming also that $CeCo_2$ and $CeFe_2$ are two-component alloys, one can estimate the lattice parameters a_2 of the second phases, which are smaller than the lattice parameters a_1 of the main phases. Generally the CeM_2 samples can be considered as a special kind of "alloy". The qualitative calculations presented here, based on the Anderson model and using this argument, lead to the appearance of the mentioned valence anomaly in $CeNi_2$, which is in qualitative agreement with our measurements.

The second suggestion is based on Wohlleben's postulation of a "dynamic alloy" [1, 5]. Using this approach to calculate the valence of the Ce ion, assuming a temperature dependence of the fluctuation temperature T_f, an anomalous behaviour of valence *vs.* temperature can also be found. In this work the valence change is assumed to be proportional to the change in the lattice parameter, Δa, of the Ce alloy with respect to the reference YNi_2. The form of the temperature dependence of T_f, which fits the measured valence, is very similar to that of the temperature dependence of the thermal expansion coefficient Δa. Hence it would seem that the fluctuation temperature T_f is strongly correlated with the thermal expansion of the lattice, in agreement with the results of ref. 1.

2. Sample preparation

The alloys studied (YCo_2, YNi_2, $CeFe_2$, $CeCo_2$, $CeNi_2$) were prepared by argon arc melting of the constituent metals, remelted several times and then homogenized at 600 °C for 2 days, at 700 °C for 2 days and finally at 800 °C for 1 week.

X-ray diffraction patterns confirm that the compounds YCo_2, YNi_2 and CeM_2 (M ≡ Fe, Co, Ni) crystallize in the cubic $MgCu_2$ structure. All the diffraction peaks of the $CeCo_2$ and $CeNi_2$ samples between $T = 4.2$ K and room temperature are asymmetrical (Fig. 1). The

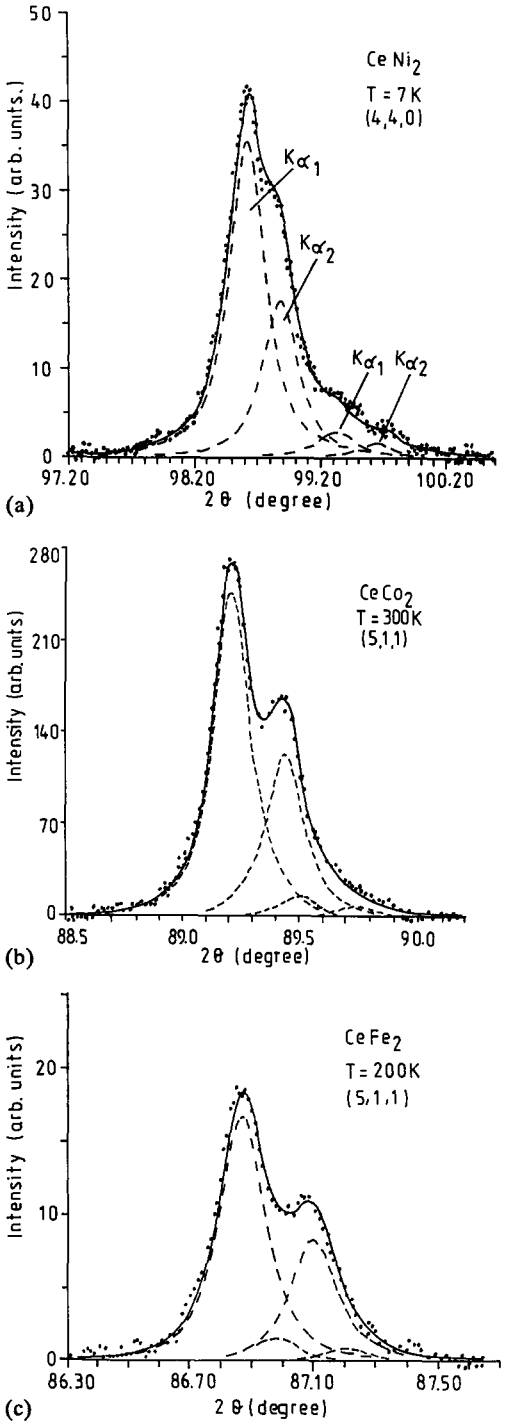

Fig. 1. Pearson-type distribution of the symmetrical $K\alpha_1$ and $K\alpha_2$ lines compared with the experimental profiles for (a) the (440) Bragg line of $CeNi_2$ at $T = 7$ K, (b) the (511) diffraction line of $CeCo_2$ measured at room temperature and (c) the (511) line of $CeFe_2$ at $T = 200$ K. The R factor equals 7% in all cases. Weak lines located near the main maximum are identified with the second phases in the $CeFe_2$, $CeNi_2$ and $CeCo_2$ alloys.

Bragg lines of $CeFe_2$ show a pronounced asymmetry at liquid nitrogen and liquid helium temperatures (Fig. 1).

3. Structural investigations

All the measurements were performed with an X-ray powder diffractometer using Fe Kα radiation. To obtain the profile of a line at room temperature and below, every reflection was measured by a scan method in which the counter was moved in steps of 0.01° and the counting time for each point was 10 s. Next the measured intensity lines were approximated by Pearson's function (VII type) [6]

$$I_i(\text{calc}) = \sum_k I_{ok}\left[1+(2^{1/m_k}-1)\left(\frac{2\Theta_{ok}-2\Theta_i}{\Delta_k/2}\right)^2\right]^{-m_k} \quad (1)$$

where I_{ok} is the maximum intensity at $2\Theta_{ok}$ for each of the k lines in the region of overlap, $2\Theta_{ok}$ is the calculated position of the Bragg peak corrected for the zero-point shift of the counter, Δ_k is the halfwidth at half-height and m_k is the shape factor. The full width 2Δ is Θ dependent and the following relation given by Cagliotti *et al.* [7] was assumed:

$$(2\Delta)^2 = A\tan^2\Theta + B\tan\Theta + C \quad (2)$$

This formula also takes into account the peak broadening resulting from the particle size effect.

The asymmetrical peaks observed in the CeM_2 diffraction patterns at room temperature and below indicate the presence of a second Ce–M phase of the $MgCu_2$ structure with very similar lattice parameters. Since the structural differences between the two phases are small, a more sophisticated method was applied for analysis of the profile of the diffracted lines.

In our case the best results were obtained in the interval $1<m<2$. For the Kα_2 profile the intensity was taken as one-half of that for the Kα_1 profile, while all other parameters were the same as used in the Kα_1 profile. Pearson-type distributions were fitted to the experimental profiles by a least-squares method. The programme for minimizing the difference

$$R = \sum_i \frac{1}{\sigma_i^2}[I_i(\text{exp}) - I_i(\text{calc})]^2 \quad (3)$$

where σ_i is the standard deviation of I_i(exp), uses the non-linear least-squares procedure employed in MINSQ [8]. The calculations do not take into account the preferred orientation correction. This effect appears to be small when a flat sample holder is used in X-ray diffraction. The best fit to the form of every (*hkl*) line for CeM_2 with deviation less than 10% was obtained by considering two symmetrical Kα_1 components of nearly lorentzian shape with the approximate intensity ratio 90:10. The same ratio of two proper Kα_2 lines in the region of overlap (Fig. 1) was assumed. The lattice constants a of the CeM_2 alloys and of the related second phases were investigated at room temperature by the Debye–Scherrer method, extrapolating $a_{hkl}(\cos^2\Theta_{ok})$ to the value corresponding to $\cos^2\Theta_k = 0$. In the plot of a as a function of atomic number of M a minimum was noted at $CeCo_2$ ($a(CeFe_2) = 7.301$ Å, $a(CeCo_2) = 7.162$ Å, $a(CeNi_2) = 7.213$ Å), which is abnormal.

We estimate the uncertainty in this experiment to be $\Delta a = 8\times10^{-4}$ Å for the lattice parameters of the main phase of CeM_2 and 2×10^{-3} Å for the second phase. The lattice constants of the second phase are $a_2(CeNi_2) = 7.193$ Å and $a_2(CeCo_2) = 7.162$ Å. For $CeFe_2$ the lattice parameter of the second phase (a_2) was not identified at room temperature, because all the diffraction lines of the diffraction pattern were nearly symmetrical. However, at lower temperatures the lines became asymmetrical. Calculation of the lattice parameter of the second phase was possible in this case, *e.g.* at 200 K the numerical deconvolution procedure of every Bragg line gave the lattice parameter a_2 as smaller than a_1 by about 0.007 Å. Unfortunately, in $CeFe_2$ the synonymous interpretation of the diffraction (*hkl*) lines seems to be more difficult. $CeFe_2$ is ferromagnetically ordered below $T_c = 235$ K [9] and the magnetostriction volume effects [10] observed below the Curie temperature also suggest tetragonal distortion.

For determining the lattice constant a_{hkl} as a function of T, only one (*hkl*) line was used. The sample was cooled in a conventional ^{4}He continuous flow cryostat. The temperature was controlled to within ±0.3 K for each diffraction peak scan.

Figure 2 shows a_{hkl} as a function of temperature for $CeFe_2$, $CeCo_2$ and $CeNi_2$. The broken curve shows the temperature dependence of the lattice constant as predicted by the Debye theory, where the coefficient of linear thermal expansion is given by

$$\alpha_L = \frac{K_L\gamma_L c_L}{3V} \quad (4)$$

Here c_L is the specific heat and K_L and $\gamma_L = \mathrm{d}(\ln\Theta_D)/\mathrm{d}(\ln V)$ are the isothermal compressibility and Grüneisen constant respectively. It is assumed that the crystal lattice parameters (K_L, γ_L) are temperature independent and $K_L\gamma_L/3V = \alpha_{exp}/c_L = A$ at room temperature, while $\alpha_{exp}(T) = c_L(T)A$ below room temperature. Below 80 K the behaviour of the compounds under study is similar and quite abnormal. The lattice parameter of CeM_2 (M ≡ Fe, Co, Ni) at low temperatures exhibits an anomalous increase compared with YNi_2 [11] and also with the lattice parameter calculated using eqn. (4). (For $CeFe_2$ two abnormal changes in the lattice parameter are observed: the first at T_c is due to the magnetic transition; the second at 90 K is discussed in this work.)

The experimental uncertainty $\Delta a = 8\times10^{-4}$ Å is smaller than the lattice constant increments $\Delta a = a_{exp} - a_{calc}$. The coefficient of linear thermal expansion,

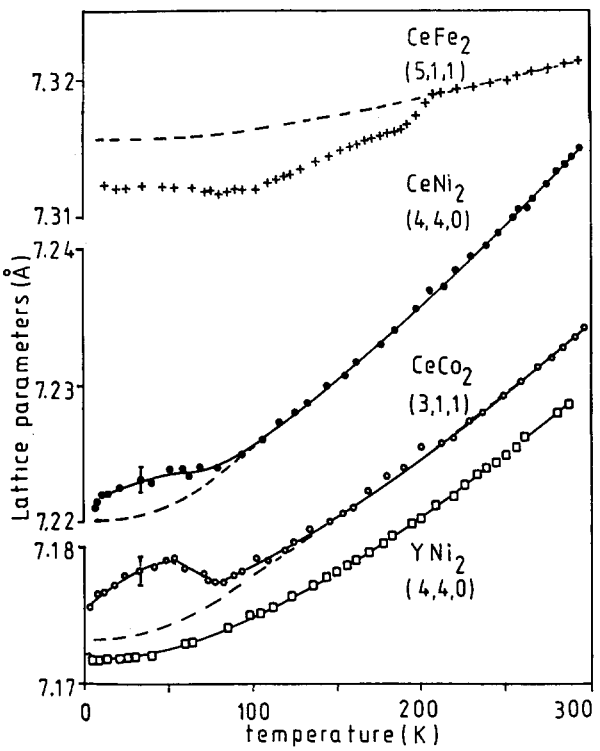

Fig. 2. Lattice parameter a of $CeFe_2$, $CeNi_2$ and $CeCo_2$ *vs.* temperature. The broken curve is calculated on the basis of eqn. (4).

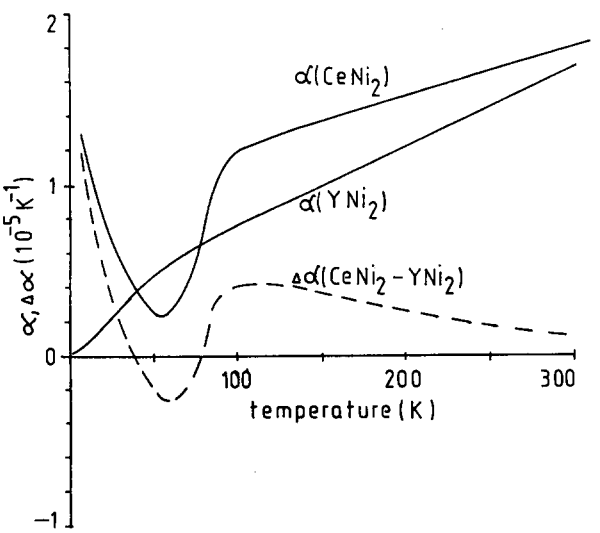

Fig. 3. Thermal expansion coefficient α of $CeNi_2$ and YNi_2 (continuous curves) and the difference $\Delta\alpha$ *vs.* temperature.

$\alpha=(1/a)\mathrm{d}a/\mathrm{d}T$, for $CeNi_2$ and YNi_2 and the difference $\Delta\alpha=\alpha(CeNi_2)-\alpha(YNi_2)$ obtained by smoothing the $a(T)$ data are shown in Fig. 3. $\Delta\alpha$ is negative between 40 and 80 K. This is typical for intermediate valent Ce (and Yb) compounds ($Ce_xLa_{1-x}Al_2$ [12], $CeAl_3$ [13], YbPd [3]), which with increasing temperature show a valence shift towards the tetravalent (trivalent) state.

The valence change of $CeNi_2$ derived from lattice constants and presented in Fig. 4 substantiates well

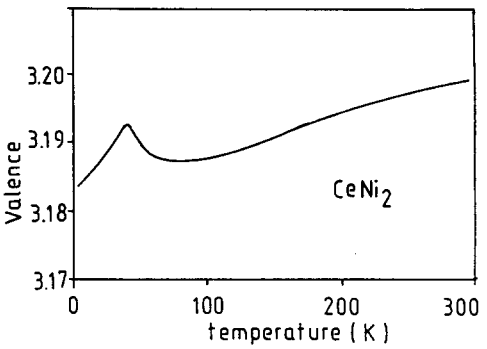

Fig. 4. Valence v *vs.* temperature as derived from Vegard's rule for $CeNi_2$.

the negative thermal expansion between 0 and 100 K. To obtain the curve presented in Fig. 4, the temperature dependence of the lattice constants of $CeNi_2$ and YNi_2 (reference compound) was measured. These substances have almost the same Debye temperature Θ_D, so the difference between lattice constants, $a(CeNi_2)-a(YNi_2)$, can be scaled, assuming the valence of Ce in $CeNi_2$ at $T=300$ K to be 3.20 (average value deduced from various L_{III} XAS edge measurements [2]). This procedure leads to the appearance of a pronounced cusp in the valence dependence of the Ce ion in $CeNi_2$ *vs.* temperature, which is seen in Fig. 4. It is noteworthy that both the intensity of the weak line numerically separated from the (*hkl*) diffraction line and its diffraction angle observed in $CeNi_2$ and $CeCo_2$ show a similar temperature dependence. These results suggest the existence of an additional CeM_2 phase of the $MgCu_2$ type. Previous structural investigations of $CeNi_2$ [14] show the collapse of the volume of a unit cell as a function of the stoichiometric composition. This study indicated a very sharp step of the order of 0.02 Å in the lattice spacing *vs.* concentration across the phase field of $CeNi_2$. Schield *et al.*'s paper [14] suggests that the formation of high concentrations of substitutional vacancies is a general feature of cerium intermediate phases. We think that the two lattice parameters in the CeM_2 series reflect the two phases on either side of the volume collapse observed in ref. 14.

Figure 5 shows $\Delta V/V$ for CeM_2 at $T=5$ K *vs.* the valence of Ce obtained from L_{III} X-ray absorption spectra [2] at 300 K. ΔV is defined as the difference between the experimental volume of the unit cell and the calculated volume at the same temperature. The compounds show an increase in $\Delta V/V$ with increasing atomic radius of the M element, as expected.

In Fig. 6 we show the temperature dependence of the Bragg (*hkl*) line intensities I of $CeNi_2$ and $CeCo_2$. The continuous curves are calculated from the relation

$$I=I_0\exp[-2B(T)]\frac{\sin^2\Theta}{\lambda^2} \qquad (5)$$

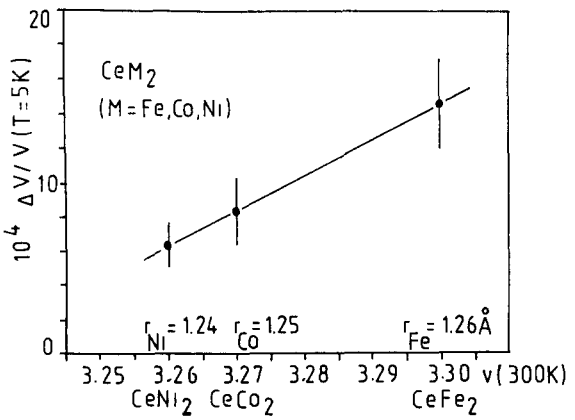

Fig. 5. Volume increment $\Delta V/V$ for $CeFe_2$, $CeCo_2$ and $CeNi_2$ at $T=5$ K *vs.* the Ce valence at 300 K.

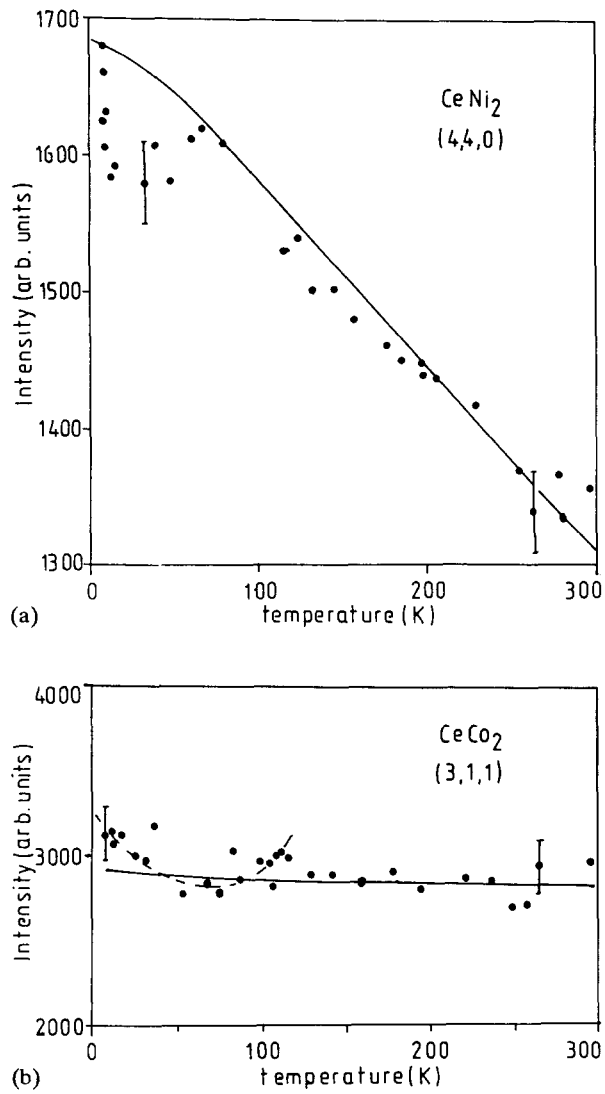

Fig. 6. Intensity of the (*hkl*) $K\alpha_1$ Bragg line *vs.* temperature for (a) $CeNi_2$ and (b) $CeCo_2$. The calculated intensities *vs.* T are presented as curves.

where $\sin^2\Theta(T)/\lambda^2=\frac{1}{4}(h^2+k^2+l^2)/a^2_{calc}(T)$; the calculated curve is normalized to the experimental one at 300 K. In terms of the Debye lattice vibration model the Debye–Waller factor was calculated from

$$B(T)=\frac{6h^2T}{k_B\bar{m}\Theta_D^2}\left[\Phi\left(\frac{\Theta_D}{T}\right)+\frac{\Theta_D}{4T}\right] \tag{6}$$

$$\Phi\left(\frac{\Theta_D}{T}\right)=\Phi(x)=\frac{1}{x}\int_0^x\frac{y\,dy}{e^y-1} \tag{7}$$

where $\bar{m}$ is the average atomic mass and Θ_D is the Debye temperature, which for $CeNi_2$ and $CeCo_2$ is known from low temperature specific heat investigations [15]. Uncertainty bars in Fig. 6 equal to the R value (10%) of the intensity of the (*hkl*) line at all T were assumed. Both $CeNi_2$ and $CeCo_2$ show a deviation between the calculated and measured intensities below 80 K, which can be interpreted as being due to a change in the Ce valence. These results are in good agreement with the lattice thermal expansion measurements.

The intensity I_0 is proportional to the square of the modulus of the structure factor F of CeM_2 given by

$$F^{(hkl)}=f_{Ce}^{(hkl)}\sum_{n=1}^{8}\exp[2\pi i(hu_n+kv_n+lw_n)]$$
$$+f_M^{(hkl)}\sum_{j=1}^{16}\exp[2\pi i(hu_j+kv_j+lw_j)] \tag{8}$$

where f_α is the atomic scattering factor. As proof, we calculated the average valence of $Ce^{3+\nu}$ in CeM_2 at room temperature by a least-squares method (eqn. (2)) comparing the calculated structure factors (8) multiplied by $\exp(-B\ \sin^2\Theta/\lambda^2)$, which include $f_{Ce^{3+\nu}}=f_{Ce^{3+}}-(f_{Ce^{3+}}-f_{La^{3+}})\nu$ (ν is the fractional occupation of $4f^0$), and the experimental structure factor $F_{exp}=(I_{exp}/pL_p)^{1/2}$, where p and L_p are multiplicity and Lorentz polarization factors respectively. The scale factor $K=\Sigma_{hkl}|F|_{exp}/\Sigma_{hkl}|F|_{calc}$ was taken as the same for all reflections in every numerical step of the programme. For the transition metals the real and imaginary components of the f correction for the anomalous dispersion effect of Fe $K\alpha$ radiation near the atomic absorption edge were used. The X-ray diffraction experiment gives $\nu=0.22$ for $CeNi_2$ and $\nu=0.32$ for $CeFe_2$, which appear to be in good agreement with L_{III} X-ray absorption measurements where values of 0.26 and 0.30 respectively were found.

4. Electrical resistivity

The electrical resistivity was measured in the temperature range between 4.2 K and room temperature

by the Van der Pauw (d.c.) method. Figure 7 shows the measured resistivities of the reference compounds YCo_2 and YNi_2 and also of $CeCo_2$ and $CeNi_2$. The results are in agreement with recently published experimental data [11, 16–18]. The resistivity of $CeCo_2$ is similar to that of $CeNi_2$ (and of $CeFe_2$ below the Curie temperature [16]). Unlike YNi_2, the electrical resistivity of YCo_2 exhibits a fairly large temperature variation. This anomalous resistivity, which is distinct from the weakly Pauli paramagnetic YNi_2 [19], may reflect the nearly ferromagnetic character of YCo_2 [20]. When the Co content in the Y–Co compounds is sufficiently large (as is the case in the concentration range from YCo_3 to Y_2Co_{17}), they become magnetically ordered.

The resistivity of YCo_2 follows a T^2 law below 20 K. The T^2 law and the high temperature saturation of ρ for YCo_2 were interpreted in terms of spin fluctuation theory [21].

On the other hand, the resistivity after subtraction of the residual resistivity ($\rho-\rho_0$) for $CeCo_2$ and $CeNi_2$ also shows a T^2 dependence below 20 K (Fig. 7), while the coefficient at T^2 is smaller than that of YCo_2 ($\Delta\rho/\Delta T^2 \approx 2.5\times10^{-2}$ $\mu\Omega$ cm K^{-2} [18]) and equal to 1×10^{-2} $\mu\Omega$ cm K^{-2}.

The form of $\Delta\rho=\rho(CeM_2)-\rho(YM_2)$ can also be predicted by Wohlleben's "dynamic alloy" model [5]. The increments $\Delta\rho/\nu$ for each CeM_2 compound are of almost the same order ($\Delta\rho/\nu=4$ $\mu\Omega$ cm $\%^{-1}$) at higher temperatures, which is in good agreement with the value $\Delta\rho_{3,4}/\nu\approx10$ $\mu\Omega$ cm $\%^{-1}$ observed for the most diluted Ce alloys [5, 22].

Figure 8 shows the resistivity increments $\Delta\rho=\rho(CeM_2)-\rho(YM_2)$ as a function of T for the CeM_2 alloys, which are similar in form to the resistivity of $CeSn_3$ [23]. The inflection temperature T_{inf} is often comparable with the inverse of the valence fluctuation lifetime (τ_f) [24] or with the spin fluctuation temperature T_f in the Fermi liquid model.

For both $CeCo_2$ and $CeNi_2$ the inflection temperature $T_{inf}\approx80$ K. It is noteworthy that *T_{inf} coincides well with the temperature below which abnormal behaviour of the lattice parameters of CeM_2 is observed* (Figs. 1–3) but is not comparable with the temperature T_{max} corresponding to the susceptibility maximum ($T_{max}\gg T_{inf}$). This disagreement has been reported previously [25]. It was also concluded [21] that T_{inf} in the $\rho(T)$ curve cannot be attributed to a crystal field effect when $T_{inf}\ll T_{max}$. In strongly mixed valent compounds the crystal field excitations are resolved only if the quasi-elastic linewidth $\Gamma_{QE}/2$ arising from inelastic neutron

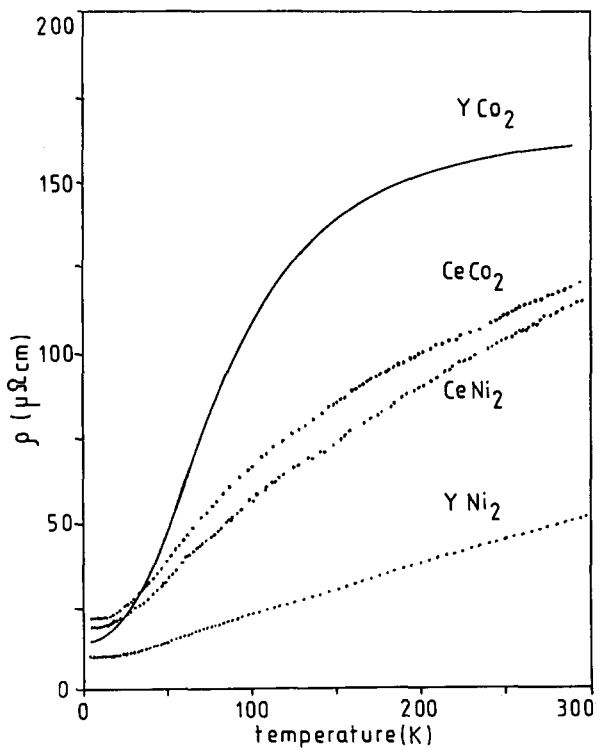

Fig. 7. Total resistivity *vs.* temperature for RM_2 samples (R ≡ Y, Ce; M ≡ Co, Ni).

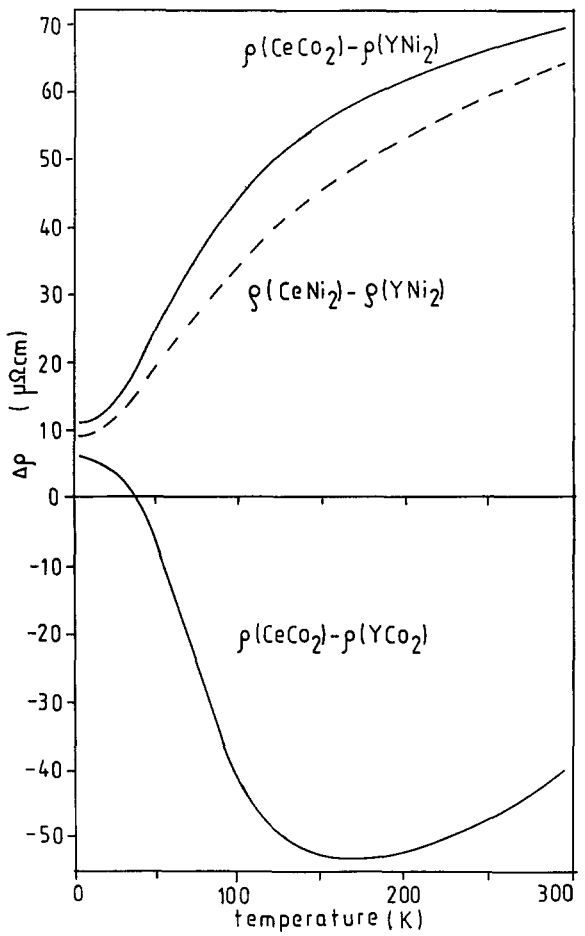

Fig. 8. Resistivity increment $\Delta\rho$ of $CeNi_2$ and $CeCo_2$ corrected by the resistivity of YNi_2 and YCo_2 respectively *vs.* temperature.

scattering of the lowest multiplet ($\Gamma_{QE}/2 = k_B T_f$ [26]) is significantly smaller than the 4f crystal field splitting Δ_{CF}. In $CeNi_2$, Δ_{CF} is of the order of 300 K [27], *i.e.* Δ_{CF} is comparable with or smaller than $\Gamma/2 \approx 400$ K (Gottwick *et al.* [17]).

It is endeavoured to connect the inflection point with the structural properties of $CeNi_2$ (CeM_2), which depend on the change in valence ν at liquid nitrogen and liquid helium temperatures.

5. Discussion

Measurements of the X-ray photoelectron (XPS) intensity [28] show that the compounds CeM_2 exhibit close similarity to the Kondo lattice in the coherent lattice treatment [29]. Owing to the lattice correlations, the Kondo resonance is split and a pseudogap near the Fermi level $E = E_f$ appears for temperatures below the Kondo temperature T_K.

At $T \approx T_{coh} \approx 0.1 T_K$ the coherence between individual Kondo sites leads to a situation where the 4f density of states is almost a constant and the Fermi level E_f lies between the peaks.

It is difficult to make a satisfactory estimate of the Kondo temperature T_K for CeM_2 (M ≡ Co, Ni), since the experimental data are to some extent contradictory. In ref. 30 two maxima were observed in susceptibility measurements, the first at 500 K and the second at about 1100 K.

Since the Kondo temperature is related to the temperature where the susceptibility has a maximum, we have here two Kondo temperatures. Unfortunately, thermopower measurements [31] show only one maximum in the thermopower at $T_K \approx 200$ K.

On the other hand, for concentrated Kondo systems the characteristic temperature T_0 [32] is given by the relation

$$T_0 = \frac{J\pi\mathscr{R}}{3\gamma} = \frac{T_K}{W_j} \tag{9}$$

where $J = \frac{5}{2}$ (Ce), γ is the linear coefficient of specific heat and W_j is the Wilson number. The characteristic temperature T_0 is related to the Kondo temperature for the $J = \frac{1}{2}$ case by $T_K = 1.2902 T_0$ [33, 34]. For small crystal field splitting ($\Delta_{CF} \ll T_K$) the total moment J contributes to the Kondo-like process. Hewson and Rasul [35] deduced that the Wilson number increases with increasing J value. Schlottmann [34], however, derived for $J = \frac{3}{2}$ and $\frac{5}{2}$ just the opposite situation, since W_j decreases for $J \geqslant \frac{3}{2}$. For the case $J = \frac{5}{2}$ the Wilson number W_j obtained in ref. 34 is 1.34627. Estimations give $T_0 \approx 680$ K [32] for $\gamma = 0.032$ J mol^{-1} K^{-2} [36].

From (9) the Kondo temperature can be estimated as $T_K \approx 915$ K, hence the coherence temperature T_{coh} for CeM_2 should be about 92 K. The value of $T_{coh} \approx 92$ K may be identified with the temperature at which anomalies in the lattice parameter and resistivity are observed.

The arguments used are only of a speculative nature and do not take into account the fact that the CeM_2 samples show two lattices with the same $MgCu_2$ structure but with different lattice constants. To support this point of view, a simple qualitative calculation may be done using the Anderson model [37].

The hamiltonian of the model has the form

$$\mathscr{H} = \mathscr{H}_0 + \mathscr{H}_1 \tag{10}$$

where

$$\mathscr{H}_0 = E_f \sum_{i,\sigma} n^f_{i\sigma} + U \sum_i n^f_{i+} n^f_{i-} + t \sum_{i,\sigma} n^c_{i\sigma} + \sum_{\substack{i,j,\sigma \\ (i \neq j)}} t_{ij} c^+_{i\sigma} c_{j\sigma} \tag{11}$$

and

$$\mathscr{H}_1 = V \sum_{i,\sigma} (f^+_{i\sigma} c_{i\sigma} + c^+_{i\sigma} f_{i\sigma}) \tag{12}$$

Here E_f is the position of the 4f level, U is the Coulomb repulsion, t is the position of the centre of gravity of the conduction band, t_{ij} is the hopping integral and V is the hybridization parameter responsible for the transfer of the 4f electron to the conduction band and vice versa. The annihilation (creation) operators related to the 4f level and conduction band are denoted by $f_{i\sigma}$ ($f^+_{i\sigma}$) and $c_{i\sigma}$ ($c^+_{i\sigma}$) respectively.

The calculation has been performed for the paramagnetic phase of the model (11) ($U = \infty$) and for an average number of electrons per atom of $n = 1.5$ (metallic state) in order to simulate qualitatively a metallic paramagnet such as $CeNi_2$.

The chemical potential μ can be found using the equation

$$n_f + n_c = n \tag{13}$$

where $n_{f,c} = \Sigma \langle n^{f,c}_\sigma \rangle$ and $\langle n^{f,c}_\sigma \rangle$ denote the thermally averaged occupation numbers with spin σ for the 4f level and conduction band respectively.

Figure 9 shows the temperature dependence of the average occupation of the conduction band, n_c, for several positions of the 4f level E_f. At the same time n_c can be identified with the valence ($v = 4 - n_f$ and $n_f = n - n_c$).

The average occupation n_c is markedly influenced by the hybridization parameter V and increases (for a given E_f) as the hybridization parameter increases.

The dependence of n_c on the bandwidth of the conduction band, W (the other parameter constant), is not so marked. As W increases up to a critical value,

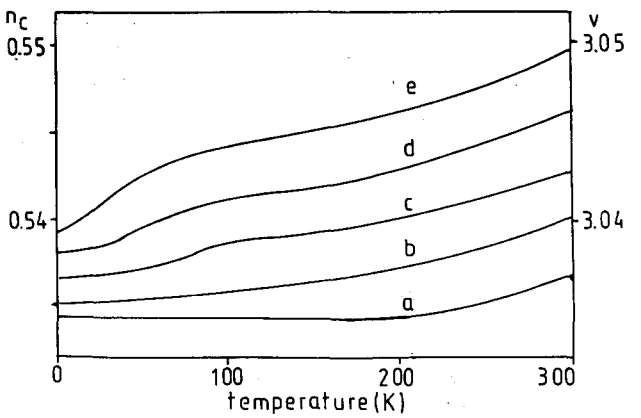

Fig. 9. Occupation number n_c of the conduction band and valence v *vs.* temperature for various positions of the 4f level E_f (eV): a, −0.6; b, −0.59; c, −0.58; d, −0.57; e, −0.56. The other parameters are $W=2$ eV, $V=0.2$ eV and an average number of electrons per atom of $n=1.5$.

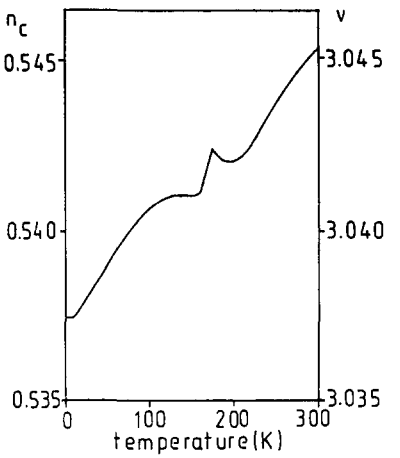

Fig. 10. Valence n_c of the hypothetical "alloy" *vs.* temperature (see (8)). Parameters (in electronvolts): $W_1=W_2=2$, $V_1=V_2=0.2$, $t_1=0, t_2=0.02, E_f=-0.57$. Average number of electrons per atom, $n=1.5$.

n_c remains constant, but when W increases further, n_c also increases. Several curves presented in Fig. 9 look similar to the experimental curve in Fig. 4, except for the more pronounced peak seen in the experiment. This peak may, however, be caused by the suggested two-phase state in the sample. To examine such a possibility, the Anderson model (10) is applied again, but for a two-component alloy. Really, the experiment suggests that the $CeNi_2$ sample is a "mixture" of two phases with different lattice constants. Therefore it is reasonable to assume that each phase of the sample can be described by the model (10), but with different parameter sets (t_i, W_i, V_i) (i is the phase number; $(i=1, 2)$; E_f and $U=\infty$ are assumed to be the same for both phases. The probability of finding phase 1 in the sample is x, while the probability is $1-x$ for finding phase 2. Since it was mentioned that the sample probably contains 90% of phase 1 and 10% of phase 2, it is reasonable to assume that $x=0.9$. The chemical potential can be calculated from the condition (averaging over the "alloy" configurations)

$$x(n_f^{(1)}+n_c^{(1)})+(1-x)(n_f^{(2)}+n_c^{(2)})=n \tag{14}$$

The valence in the model is again the averaged occupation number (similarly as in (14))

$$n_c=xn_c^{(1)}+(1-x)n_c^{(2)} \tag{15}$$

where $n_{f,c}^{(1,2)}=n_{f,c}^{(1,2)}(t_{1,2}, W_{1,2}, V_{1,2})$ and these quantities can be calculated i a similar way as above.

Figure 10 shows the valence in this model as a function of temperature calculated from (15). Since the lattice constants of the two phases differ only slightly, only small differences are assumed between the parameter sets s_1 and s_2 $(s_i=t_i, W_i, V_i)$; $i=1, 2$). In fact, it is sufficient to move up the centre of gravity of the conduction band of phase 2 with respect to that of phase 1, leaving the other parameters unchanged. A peak is seen in the temperature dependence of n_c. Although our considerations are only of a qualitative nature, they lend plausibility to the hypothesis that the peak appearing in the valence temperature dependence (see Figs. 2 and 4) is an effect of "alloying". The density of states is markedly dependent on the model parameters, and when two phases are "mixed", as in (14) or (15), at a certain temperature a peak due to the different shapes of the densities of states of the "alloy" components appears.

The magnetic susceptibility of such an "alloy" may also be considered. In this case the calculated susceptibility will show two pronounced maxima similar to those observed by experiment [30]. It is evident that the anomalies in the valence and susceptibility are due to the existing "substructure" of the sample, even in the case where the parameters of the Anderson model are far from the Kondo regime.

Another approach may be postulated based on the "dynamic alloy" theory. Here the valence ν of the Ce ion in a compound is described by the formula [38]

$$\nu=\left\{1+\left[2+4\exp\left(\frac{-\Delta_{CF}}{T+T_f}\right)\right]\exp\left(\frac{-E_x}{T+T_f}\right)\right\}^{-1} \tag{16}$$

where E_x is the interconfigurational excitation energy $(E_x=E_{n+1}-E_n)$ and $T_f=T_f(T)$ is the fluctuation temperature. Formula (16) gives a good fit to our experimental curve (Fig. 4) on assuming the T_f temperature dependence presented in Fig. 11. The parameters Δ_{CF} and E_x are only very weakly dependent on T and assumed here to be constant.

On comparing the T_f temperature dependence (Fig. 11) and $\Delta\alpha(T)$ (Fig. 3), it may be seen that in the "dynamic alloy" theory these two quantities are very strongly correlated. In other words, the phenomeno-

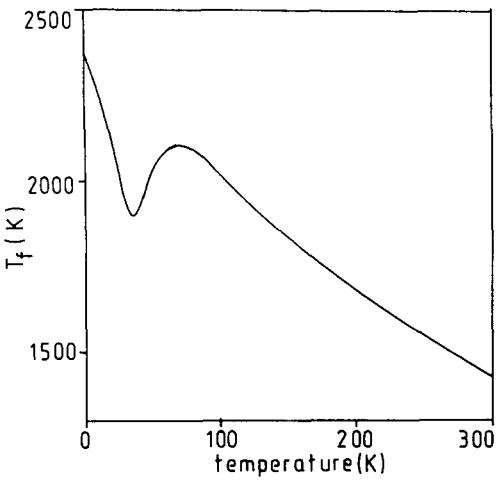

Fig. 11. Temperature dependence of the fluctuation temperature T_f which fits, using (9), the experimental curve (Fig. 4). Parameters (in kelvins): $\Delta_{CF}=300$, $E_x=500$.

logical fluctuation temperature T_f is strongly correlated with the volume temperature dependence of the sample. Here the two-component "alloy" approach presented above can also be applied. Then instead of (16) we should write

$$\nu=0.9\nu^{(1)}+0.1\nu^{(2)} \tag{17}$$

with $\nu^{(i)}=\nu^{(i)}(\Delta_{CF}^{(i)}, E_x^{(i)}, T_f^{(i)})$ $(i=1, 2)$. This approach, when fitted to our curve (Fig. 4), leads to a $T_f^{(1,2)}$ temperature behaviour similar to that presented in Fig. 11.

6. Conclusions

(1) The shape of the diffraction lines in the CeM_2 (M ≡ Fe, Co, Ni) samples suggests that these substances can be considered as a combination of two $MgCu_2$ structures with two different lattice constants a_1 and a_2 $(a_1>a_2)$. The ratio of the numbers of crystal unit cells belonging to the two different phases is $N(a_1)/N(a_2)=9$.

(2) The CeM_2 samples are considered in this work as a special kind of "alloy".

(3) As proof, the average valences of Ce ions in CeM_2 were calculated at room temperature by X-ray diffraction experiments, comparing the experimental and calculated structure factors. Good agreement between the results obtained by the X-ray diffraction method and L_{III} XAS edge was noted.

(4) The lattice parameter of CeM_2 (M ≡ Fe, Co, Ni) investigated as a function of T exhibits below about 80 K an anomalous increase compared with YNi_2. This behaviour is similar for the compounds under study and is abnormal. Moreover, for $CeFe_2$ the next abnormal behaviour of the lattice parameter connected with the magnetic phase transition at the Curie temperature was observed. The abnormal change in the volume of CeM_2 at low temperatures is explained here by the valence change of the Ce ion. Both the negative value of the lattice thermal expansion coefficient and the abnormal decrease in the intensities of the diffraction lines in CeM_2 observed at low temperatures confirm that the valence of Ce in the "alloy" changes.

(5) A quantitative explanation of the abnormal variation in the Ce ion valence with temperature is proposed on the basis of the Anderson model applied to an "alloy" defined as a mixture of two different CeM_2 phases.

References

1 J. Röhler, D. Wohlleben, J.P. Kappler and G. Krill, *Phys. Lett. A, 103* (1984) 220.
2 J. Röhler, in K.A. Gschneidner Jr., L. Eyring and S. Hufner (eds.), *Handbook on the Physics and Chemistry of Rare Earths*, Vol. 10, Elsevier, Amsterdam, 1987, Table 3, pp. 488–489.
3 R. Pott, W. Boksch, G. Leson, B. Politt, H. Schmidt, A. Freimuth, K. Keulertz, J. Langen, G. Neumann, F. Oster, J. Röhler, U. Walter, P. Widener and D. Wohlleben, *Phys. Rev. Lett., 54* (1985) 481.
4 D. Malterre, *Phys. Rev. B, 43* (1991) 1391.
5 D. Wohlleben and B. Wittershagen, *Adv. Phys., 34* (1985) 403.
6 A. Ratuszna and K. Majewska, *Powder Diffract., 5* (1990) 41.
7 G. Cagliotti, A. Pauletti and F.P. Ricci, *Nucl. Instrum., 3* (1958) 223.
8 T. Pomentale, MINSQ-*Program for Minimizing of a Sum of Squares of a Function*, CERN Computer Centre Program Library, Geneva, 1968.
9 K.H.J. Buschow, *Rep. Prog. Phys., 40* (1977) 1179.
10 M. Sigha, Y. Muraoka and Y. Nakamura, *J. Magn. Magn. Mater., 10* (1979) 280; W. Zarek, personal communication.
11 A. Ślebarski, J. Jelonek and D. Wohlleben, *Z. Phys. B, 66* (1987) 47.
12 M. Lang, R. Schefzyk, F. Steglich and N. Grewe, *J. Magn. Magn. Mater., 63–64* (1987) 79.
13 M. Ribault, A. Benoit, J. Flouquet and J. Palleau, *J. Phys. (Paris), 40* (1979) L413.
14 T.C. Shields, J. Mayers and I.R. Harris, *J. Magn. Magn. Mater., 63–64* (1987) 587.
15 M.A. Sa', J.B. Oliveira, J.M. Machado da Silva and I.R. Harris, *J. Less-Common Met., 108* (1985) 263.
16 H.J. van Daal and K.H.J. Buschow, *Phys. Status Solidi A, 3* (1970) 853.
17 P. Scorbia, A. Harrus, B. Andraka, T. Mihalisin, S. Raaen and R.D. Parks, *J. Appl. Phys., 55* (1984) 1969; J. Sakurai, T. Ohyama and Y. Komura, *J. Magn. Magn. Mater., 63–64* (1987) 578; U. Gottwick, K. Gloos, S. Horn, F. Steglich and N. Grewe, *J. Magn. Magn. Mater., 47–48* (1985) 536.
18 K. Ikeda, *J. Phys. Soc. Jpn., 42* (1977) 1541.
19 E. Burzo and J. Laforest, *Int. J. Magn., 3* (1972) 171.
20 R. Lemaire, *Cobalt, 33* (1966) 201; E. Burzo, *Int. J. Magn., 3* (1972) 161; K. Ikeda, K.A. Gschneidner Jr., R.J. Stierman, T.W.E. Tsang and D.D. Mcmasters, *Phys. Rev. B, 29* (1984) 5039.

21 K. Ueda and T. Moriya, *J. Phys. Soc. Jpn., 39* 91975) 605.
22 A. Ślebarski and D. Wohlleben, *Z. Phys. B, 60* (1985) 449.
23 T. Stalinski, Z. Kletowski and Z. Henkie, *Phys. Status Solidi A, 19* (1973) K165.
24 B.C. Sales and D. Wohlleben, *Phys. Rev. Lett., 35* (1975) 1240.
25 A. Mauger, V. Paul-Boncour, M. Escorne, A. Percheron-Guegan, J.C. Achard and J. Darriet, *Phys. Rev. B, 41* (1990) 2307.
26 E. Holland-Moritz, D. Wohlleben and M. Loewenhaupt, *Phys. Rev. B, 25* (1982) 7482; E. Holland-Moritz, *J. Magn. Magn. Mater., 47–48* (1985) 127; D. Wohlleben and B. Wittershagen, *J. Magn. Magn. Mater., 52* (1985) 32.
27 W.E. Wallace, S.G. Sankar and V.U.S. Rao, in J.D. Dumitz, P. Hammerich, J.A. Ibers, C.K. Jorgensen, J.B. Neilands, D. Reinen and R.J.P. Williams (eds.), *Structure and Bonding,* Vol. 33, Springer, Berlin/Heidelberg, 1977, p.1.
28 J.W. Allen, S.J. Oh, O. Gunnarsson, K. Schönhammer, M.B. Maple and M.S. Torikachvili, *Adv. Phys., 35* (1986) 275.
29 H. Koga and H. Kubo, *Physica B, 147* (1987) 205; *Solid State Commun., 65* (1988) 257; H. Koga, H. Kubo and T. Fujiwara, *Phys. Rev. B, 37* (1988) 341.
30 G.L. Olcese, *Solid State Commun., 35* (1980) 87.
31 J. Sakurai, T. Ohyama and Y. Komura, *J. Magn. Magn. Mater., 63–64* (1987) 578.
32 N.B. Brandt and V.V. Moshchalkov, *Adv. Phys., 33* (1984) 373.
33 N. Andrej and J.H. Lowenstein, *Phys. Rev. Lett., 46* (1981) 356.
34 P. Schlottmann, *Z. Phys. B, 51* (1983) 223.
35 A.C. Hewson and J.W. Rasul, *J. Phys. C: Solid State Phys., 16* (1983) 6799.
36 B. Andraka, J. Timlin and T. Mihalisin, *J. Magn. Magn. Mater., 47–48* (1985) 96.
37 P.W. Anderson, *Phys. Rev., 124* (1961) 41.
38 D. Wohlleben in J.V. Acrivos *et al.* (eds.), *Physics and Chemistry of Electrons and Ions in Condensed Matter,* Reidel, Dordrecht, 1984, p. 85.